Editors' Suggestion | Featured in Physics

Coexistence of Photoelectric Conversion and Storage in van der Waals Heterojunctions

Yucheng Jiang,[1,*] Anpeng He,[1,‡] Run Zhao,[1] Yu Chen,[1] Guozhen Liu,[1] Hao Lu,[1] Jinlei Zhang,[1] Qing Zhang,[2] Zhuo Wang,[3] Chen Zhao,[2] Mingshen Long,[4] Weida Hu,[4] Lin Wang,[5] Yaping Qi,[6] Ju Gao,[1,7] Quanying Wu,[1] Xiaotian Ge,[8] Jiqiang Ning,[8] Andrew T. S. Wee,[9] and Cheng-Wei Qiu[2,†]

[1]*Jiangsu Key Laboratory of Micro and Nano Heat Fluid Flow Technology and Energy Application, School of Physical Science and Technology, Suzhou University of Science and Technology, Suzhou, Jiangsu 215009, People's Republic of China*
[2]*Department of Electrical and Computer Engineering, National University of Singapore, Singapore 117583, Singapore*
[3]*International Collaborative Laboratory of 2D Materials for Optoelectronics Science and Technology of Ministry of Education, Institute of Microscale Optoelectronics, Shenzhen University, Shenzhen 518060, China*
[4]*State Key Laboratory of Infrared Physics, Shanghai Institute of Technical Physics, Chinese Academy of Sciences, 500 Yu Tian Road, Shanghai 200083, China*
[5]*School of Materials Science and Engineering, Shanghai University, Shanghai 200444, China*
[6]*Purdue Quantum Science and Engineering Institute, Purdue University, West Lafayette, Indiana 47907, USA*
[7]*School for Optoelectronic Engineering, Zaozhuang University, Shandong 277160, China*
[8]*Vacuum Interconnected Nanotech Workstation, Suzhou Institute of Nano-tech and Nano-Bionics (SINANO), Suzhou, Jiangsu 215123, People's Republic of China*
[9]*Department of Physics, National University of Singapore, Singapore 117551, Singapore*

(Received 15 January 2020; revised 2 June 2021; accepted 27 September 2021; published 19 November 2021)

Van der Waals (vdW) heterojunctions, based on two-dimensional (2D) materials, have great potential for the development of ecofriendly and high-efficiency nanodevices, which shows valuable applications as photovoltaic cells, photodetectors, etc. However, the coexistence of photoelectric conversion and storage in a single device has not been achieved until now. Here, we demonstrate a simple strategy to construct a vdW *p-n* junction between a WSe_2 layer and quasi-2D electron gas. After an optical illumination, the device stores the light-generated carriers for up to seven days, and then releases a very large photocurrent of 2.9 mA with bias voltage applied in darkness; this is referred to as chargeable photoconductivity (CPC), which completely differs from any previously observed photoelectric phenomenon. In normal photoconductivity, the recombination of electron-hole pairs occurs at the end of their lifetime; in contrast, infinite-lifetime photocarriers can be generated and stored in CPC devices without recombination. The photoelectric conversion and storage are completely self-excited during the charging process. The ratio between currents in full- and empty-photocarrier states below the critical temperature reaches as high as 10^9, with an external quantum efficiency of 93.8% during optical charging. A theoretical model developed to explain the mechanism of this effect is in good agreement with the experimental data. This work paves a path toward the high-efficiency devices for photoelectric conversion and storage.

DOI: 10.1103/PhysRevLett.127.217401

Photoelectric conversions, such as photoconductive and photovoltaic effects, often occur in *p-n* junction systems, where incident photons create electron-hole pairs (EHPs) [1,2]. For high-performance devices, it is necessary to achieve high photoelectric efficiency and electron-hole separations [3]. However, the rapid recombination of EHPs tends to shorten the lifetime of photocarriers, therefore, limiting external quantum efficiency (EQE) [4,5]. Many strategies have been proposed to obtain efficient photoelectric devices by searching for novel *p*- and *n*-type materials or designing a functional interface structure [6–9]. Basic methods of realizing high EQE involve the improvement of the trapping or absorption of photons, e.g., surface plasmon excitation and element doping; few studies have focused on extending the lifetime of photocarriers [10–15]. Recent advances in Van der Waals (vdW) heterojunctions have created new potential for the development of high-performance photoelectric devices [16–22]. Based on 2D layered materials, the vdW heterostructures give rise to attractive possibilities for manipulating the generation, recombination, and transport of photocarriers in atomic interfaces [16,20,21,23,24]. Several notable photoelectric properties have been reported by facilitating the design of atomically thin devices, such as photocatalysis [19], photoconductivity [22,25], photovoltaic effect [26–28], and electroluminescence [29]. A strong advantage is that the layer-dependent band structure allows the physical properties of the *p-n* junction to be controlled without creating extra disorder [30]. However, until now, most of the vdW junctions have been mainly

structured by n- or p-type 2D layered materials [20]. Another 2D system, 2D electron gas, has been extensively studied because of its abundant physical properties [31–33], but no effort has been made to construct p-n junctions based on it.

In this Letter, we develop a practical Ar^+-ion-bombardment assistant (AIBA) method to establish a lateral vdW p-n junction between few-layered WSe_2 and quasi-2D electron gas (Q2DEG) on $SrTiO_3$ (STO). The chargeable photoconductivity (CPC) effect is observed for the first time, completely differing from any previously observed photoelectric phenomenon. The device cannot only create photocarriers under optical illumination, but also store them in the space charge region, indicating the achievement of simultaneous energy conversion and storage. After seven days, a large photocurrent of 2.9 mA is released with bias applied in darkness. During this process, EHPs recombine, and the device returns to the insulating state. The ratio of currents in full- and empty-photocarrier states reaches as high as 10^9 with high EQE of 93.8%. Based on the existence of infinite-lifetime photocarriers, we propose a theoretical model to explain the mechanism of this remarkable effect, in good agreement with experimental data.

A detailed description of the AIBA method has been offered in Sec. 1 of the Supplemental Material [34]. A schematic of the WSe_2-Q2DEG heterostructure is shown in Fig. 1(a). During the fabrication, one half of few-layered WSe_2 is coated with photoresist, and the other half is irradiated by an Ar^+ ion beam (see Fig. S1 in the Supplemental Material [34]). A thin layer of oxygen vacancies will be induced by Ar^+ etching on the STO surface. The previous studies have demonstrated that oxygen vacancies can cause a high density of Q2DEG [39,40]. In this case, a vdW contact can be achieved between the edges of few-layered WSe_2 and Q2DEG. Despite indirect contact, the electric transport is still realized by the electron tunneling. Due to the p-type conduction of intrinsic WSe_2, a lateral p-n heterojunction is formed in the interface of WSe_2 and Q2DEG, exhibiting good rectifying behavior [see Fig. S2(a) in the Supplemental Material [34]]. In Fig. 1(b), an atomic-force microscopy (AFM) image shows the surface morphology of the device with the WSe_2 flake of 39.5-nm thickness. The inset is a photographic image of the selected region.

With the circuit cut off, the device is irradiated by a 405-nm, 16 mW/cm^2 laser, and the exposure time (t_e) is 6 s at 30 K, as shown in Fig. 1(a). The light is then turned off, and the device is kept in darkness for 2 min or 7 days in Fig. 1(c). Afterward, a very large photocurrent of about 2.9 mA is released with bias voltage increasing to 5 V in darkness in Fig. 1(d). This unique photoelectric phenomenon is the CPC effect. Note that the waiting process exhibited in Fig. 1(c) must be performed in a circuit cut-off state; otherwise, photocarriers will be slowly released, even at zero voltage [see Fig. S2(b) in the Supplemental Material [34]]. The device is self-excited to store photocarriers in the p-n interface under optical illumination, which is highly similar to the charging process of a battery. After optical charging, the stored photocarriers can flow across the junction under bias voltage, even with the light removed. The forward curve (voltage increase) shows a releasing process of the photocarriers, while the backward one (voltage decrease) implies a recovery process toward the deletion state of carriers. The inset in Fig. 1(d) demonstrates that the maximum current under optical illumination is 10^9 times higher than that in darkness. Within one I-V loop, the ratio of forward and backward currents is as high as 10^4 at 3 V, which demonstrates that over 99.9% of stored photocarriers recombine under bias voltage. Fig. 1(e) shows that the CPC effect originates from the existence of infinite-lifetime photocarriers in the intrinsic space charge region (ISCR). To clarify the processes of photocarrier generation and storage, we use a micro-laser-beam with 0.7-μm radius to illuminate different positions on the heterojunction (see Secs. 2 and 3 and Fig. S3 in the Supplemental Material [34]). It is found that the photocarriers stored in ISCR are photogenerated holes (PGHs)

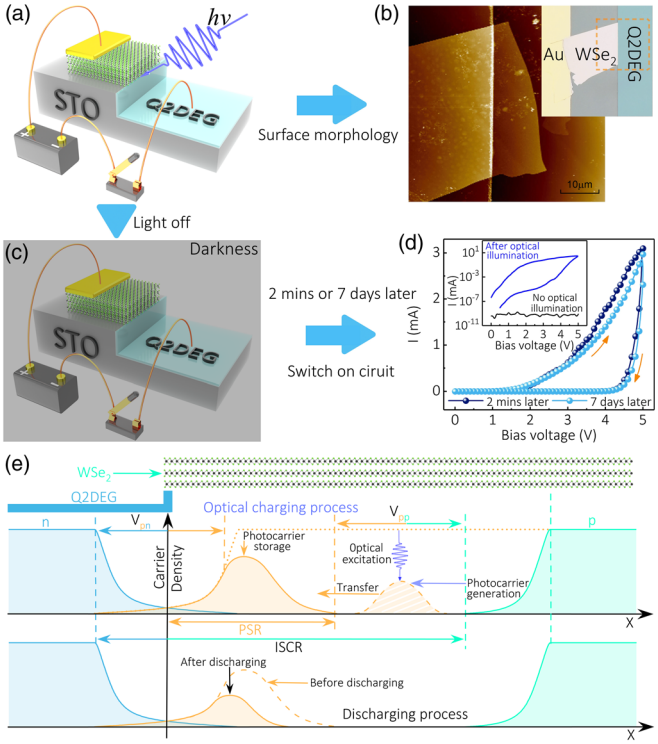

FIG. 1. (a) Schematic of WSe_2-Q2DEG heterostructure under 405-nm, 16 mW/cm^2 optical illumination. t_e is 6 s, and the circuit is cut off. (b) AFM image showing the surface morphology. Inset: photograph of the device. (c) Device placed in darkness for 2 min or 7 days at 30 K. (d) I-V loops measured in darkness 2 min later and 7 days later, respectively. Inset: I-V curves without and after optical illumination. (e) Schematic showing the generation, storage, and release of photocarriers stored in the ISCR for the optical charging and discharging.

in the region of WSe_2 (see Sec. 2 and Fig. S4 in the Supplemental Material [34]). The PGHs can fill the ISCR so as to form a photocarrier-induced pseudo-space-charge region (PPSCR). The three regions determine the electric transport of the device together, which are the n region, p region, and PGH storage region (PSR). During the optical charging, the region near the interface should be preferentially filled by PGHs, and then other regions that are gradually filled in the ISCR [see Secs. 3 and 4 and Figs. S5(a) and S5(b) in the Supplemental Material [34]]. During discharging, applying bias voltage causes the release of the PGHs stored in ISCR [see Sec. 5 and Fig. S5(c) in the Supplemental Material [34]]. In this Letter, we focus on the CPC effect at positive bias voltages, although the device can also discharge photocarriers at negative bias voltages (see Fig. S6 in the Supplemental Material [34]). It shows even higher efficiency of discharge than the positive bias (see Sec. 6 in the Supplemental Material [34]). Once the photocarriers are completely exhausted, no significant photocurrent will be obtained at positive or negative voltages. Moreover, the cycle of charge and discharge is highly repeatable. The device can maintain the same level of photocurrent even after 1000 cycles [see Fig. S7(a) in the Supplemental Material [34]].

Fig. 2(a) shows the I-V curves with different bias voltage increment rates (v_r), offering additional evidence of storage behavior. It is found that the current increases significantly with the increase of v_r, distinguished from the normal photoconductivity (NPC) such as transient and persistent photoconductivity effects. For this CPC effect, larger v_r means a stronger tendency to recombine EHPs and a shorter carrier release time. This inevitably leads to an increase in current, due to the fixed amount of stored charges with full charging. The v_r dependence of current is a key feature that can be used to distinguish CPC from NPC in experiments.

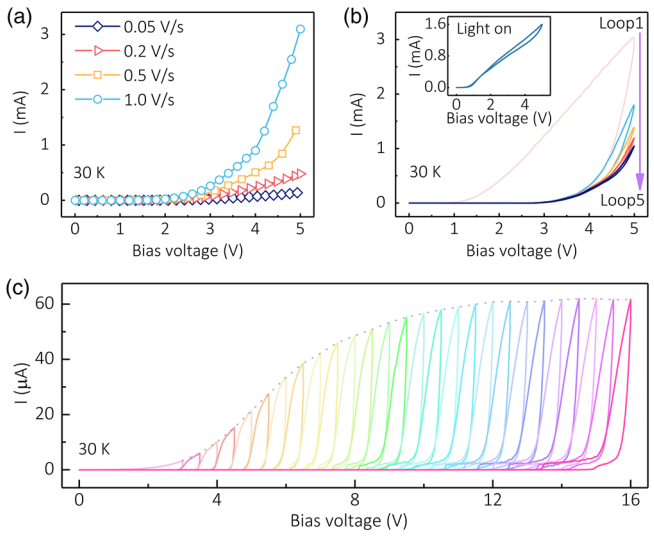

FIG. 2. (a) Dependence of photocurrent on v_r after full charging. For simplicity, only forward photocurrents are shown. (b) I-V loops in multiple circles after a single optical charge, showing the fading photocurrents as the loop number increases. Inset: I-V loop under continuous optical illumination. (c) I-V loops following several voltage ranges of 0–4 V, 0–4.5 V, 0–5 V, 0–5.5 V $\cdots$ 0–16 V in turn after a single full charging, with $v_r = 0.1$ V/s.

I-V loops are repeated 5 times after a single optical charging, as shown in Fig. 2(b). Although over 99.9% of stored photocarriers can be consumed in the first loop, residual charges are still trapped in the ISCR to prevent the device from returning to the intrinsic insulating state. Besides, the photoswitching characteristic shows fast photoelectric responses, indicating a different nature from persistent photoconductivity despite their similar ability to record optical information [see Fig. S7(b), Secs. 7 and 8 in the Supplemental Material [34]]. The response time is less than 30 ms by investigating the photocurrents with on-off light [see Fig. S8(a) in the Supplemental Material [34]]. The inset in Fig. 2(b) shows the I-V curve with a light on, compared with that in darkness after full charging. Ordinarily, for the NPC effect, photoelectric materials should exhibit the largest photocurrent under the continuous irradiation of light. However, a different phenomenon has been observed in the WSe_2-Q2DEG heterostructure, by which the discharge current measured in darkness is much larger than that under continuous optical illumination. A reasonable explanation may be offered based on the infinite lifetime of photocarriers. Without EHP recombination, the photocarriers will gradually accumulate to a high density, thus causing a large photocurrent in darkness. In contrast, with bias voltage and optical illumination applied together, the light-produced electrons and holes tend to be recombined promptly without accumulation.

At low temperature, the device has a large built-in potential over 25 V and a long ISCR with the width of 18 μm. The ISCR can act as a container to store the photocarriers. Fig. 2(c) shows I-V loops measured one by one in a series of voltage ranges from 0–4 V to 0–16 V after a single full charge. A small v_r is used to prevent damage to the device due to a large current. Intriguingly, after the stored photocarriers are completely exhausted in low voltage ranges, the device still releases a large photocurrent at higher voltages. High bias voltage may drive infinite-lifetime photocarriers, stored in deeper ISCR, to cross built-in barriers, thus contributing to the electrical transport.

Figure 3(a) illuminates photocurrent and dark currents as a function of temperature at 4 V. With temperature dropping, the WSe_2-Q2DEG heterostructure gradually loses its electric conductivity, and even acts as an insulator below 160 K. In contrast, the photocurrent tends to increase sharply as the temperature decreases to 9 K. It is noted that there exists a critical temperature ($T_c \approx 80.3$ K) below which the photocurrent exhibits a rapid increase. We use Q_{a-b} to express the charge capacity of photocarriers between the voltage levels of a and b (see Sec. 9 in the Supplemental Material [34]). Because of the insulation

after complete discharging, all of the stored charges will become the carriers collected in the electric measurement. Figure 3(b) shows the temperature dependence of Q_{0-25}. It is found that the storage capacity of photocarriers increases rapidly as temperature decreases below 80.3 K, a temperature which happens to be the same as the T_c. In order to achieve the CPC effect, two requirements have to be satisfied: electric insulation and infinite-lifetime photocarriers. WSe_2-Q2DEG heterostructures become insulating below 160 K and produce infinite-lifetime photocarriers below T_c. Actually, T_c reveals the crossover from graded to one-sided junctions, below which the lifetime of photocarriers becomes infinite and the device changes from NPC to CPC states (see Sec. 10 in the Supplemental Material [34]). The infinite lifetime mainly refers to the storage lifetime of photocarriers [see Sec. 11 and Fig. S8(b) in the Supplemental Material [34]]. In addition, the charge capacity of Q_{0-5} shows a dependence on the thickness of WSe_2 (see Fig. S9 in the Supplemental Material [34]). The 39.5-nm device shows the best CPC, and is used throughout the experiments.

Figure 3(c) shows I-V loops after full charging with different wavelengths of visible light. As expected, the short-wavelength (or high-energy) photons are more likely to transform into infinite-lifetime photocarriers in the junction. For long-wavelength (over 532 nm) visible light, the CPC effect is still significant, but is achieved only

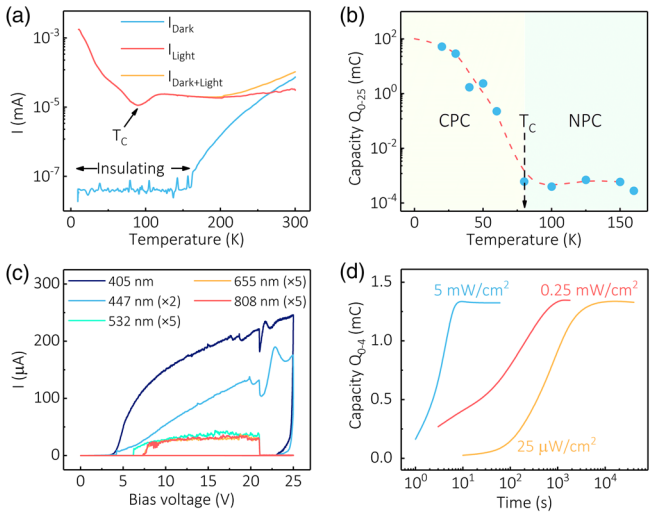

FIG. 3. (a) Temperature dependence of dark current, photocurrent, and overall current under a 1 mW/cm^2 optical illumination at 4 V. (b) Charge capacity of stored photocarriers as a function of temperature. (c) I-V loops formed by using lasers of different wavelengths to charge the device. All measurements are performed with full charging and $v_r = 0.25$ V/s. Photocurrent at 447 nm is amplified twofold, and those at 532 nm, 655 nm, and 808 nm are amplified fivefold, respectively. (d) Charge quantity of stored photocarriers versus exposure time with 405-nm light of different power densities, showing the same saturation charge quantity.

below the bias voltage of 21 V. It seems that the energies of long-wavelength photons are too low to activate the storage behavior of photocarriers at high voltage levels. With the wavelength larger than 900 nm, the CPC effect tends to disappear, which may be determined by the band gap of WSe_2 [41]. In addition, the optical charging procedure has been investigated in Fig. 3(d). Despite different optical powers, the values of Q_{0-4} can reach almost the same maximum with sufficient exposure time, suggesting full optical charging. The charging time depends strongly on the optical power density. Under a 5 mW/cm^2 optical illumination, it takes less than 6 s for the device to be fully charged. As the optical power density decreases, more time is needed for full charging. No matter how small the optical power is, the device always harvests sporadic photons and accumulates plenty of photocarriers, finally releasing a large photocurrent under bias voltages. Here, we use EQE to evaluate the charging ability of the device. The high EQE indicates the high photoelectric response [42–44]. The self-excited transition procedure from photons to infinite-lifetime photocarriers exhibits high EQE, up to 93.8% (see Sec. 9 and Fig. S10 in the Supplemental Material [34]).

To understand the CPC effect, two basic assumptions are suggested to establish a theoretical model: (i) the photocarriers cannot spontaneously recombine in ISCR and (ii) ISCR has a very large built-in potential (V_{bi}) and width, which can be regarded as a container for photocarrier storage. Through the classical theory of p-n junctions, the photocarrier density is written as $n_{ph} = G\tau$, where G is the generation rate of electron-hole pairs, and τ is the lifetime of photocarriers. However, for infinite-lifetime photocarriers in the CPC effect, the above equation needs to be modified and is expressed as $n_{ph} = Gt_e$, where t_e is the exposure or charging time. Since PGHs tend to move toward the interface [see Fig. 1(e) and Sec. 3 in the Supplemental Material], n_{ph} should be the PGH density in PSR [34]. The vdW interface and space charges tend to hold the photocarrier density steady and prevent the recombination of EHPs. As per classical theory, there should exist a photocarrier-induced pseudo-built-in potential (V_{bi}^{ph}) in PPSCR. Considering $V_{bi}^{ph} = V_{pn} + V_{pp}$ (see Sec. 5 in the Supplemental Material), I-V characteristics depend mainly on V_{bi}^{ph} [34]. Current flow causes the recombination of electron-hole pairs and consumes the PGHs in PPSCR. Since V_{bi}^{ph} is directly determined by the distribution of photocarriers stored in ISCR, the consumption of PGHs will lead to an increase of V_{bi}^{ph}. With the circuit switched on, the change of V_{bi}^{ph} should be correlated with I_{ph}. For simplicity, we assume the linear relation between I and (dV_{bi}^{ph}/dt) as

$$\frac{dV_{bi}^{ph}}{dt} = \frac{R_f}{Gt_e} I_{ph}, \tag{1}$$

where R_f is a constant, named as the recombination factor that may be correlative to the specific distribution of PGHs in ISCR.

From Eq. (1) and the theory of the p-n junction, a differential equation for the CPC effect can be formed as

$$\frac{kT}{q_e}\frac{dI_{ph}}{dt} = \frac{v_r I_{ph}}{1-\exp\left(-\frac{q_e V}{kT}\right)} - \frac{R_f}{Gt_e} I_{ph}^2, \tag{2}$$

where V is the bias voltage, q_e is the electric charge of an electron, k is the Boltzmann constant, and T is the temperature. In our experiments, V increases at a constant rate (v_r), where $V = v_r t$. Considering the initial conditions, we obtain the I-V relation as

$$I_{ph}(V, V_{bi,0}^{ph}) = \frac{I_0 v_r G t_e [\exp(\frac{q_e V}{kT}) - 1]}{I_0 R_f [\exp(\frac{q_e V}{kT}) - \frac{q_e V}{kT}] + v_r G t_e \exp(\frac{q_e V_{bi,0}^{ph}}{kT})}, \tag{3}$$

where $V_{bi,0}^{ph}$ is the initial V_{bi}^{ph}. Interestingly, this equation predicts the existence of a saturation current ($I_s = Gt_0 v_r / R_f$) at a large bias voltage. In the experiments, we decrease v_r to avoid the device breakage, and increase the upper limit of bias voltage. Fig. 4 shows the observed saturation behavior and its fitting curve. The fitting parameters used to generate the fitting curve are $I_0 = 1.3$ nA, $V_{bi,0}^{ph} = 9.8$ V, and $R_f/G = 30.8\ \Omega$. The inset in Fig. 4 exhibits the theoretical and experimental V_{bi}^{ph} as a function of V. The method to obtain V_{bi}^{ph} is shown in Secs. 12 and 13 in the Supplemental Material [34]. It is worth pointing out that R_f/G reflects the ability to release the photocarriers stored in ISCR. The theoretical simulation is highly consistent with the experimental data, supporting our theoretical model for the CPC effect.

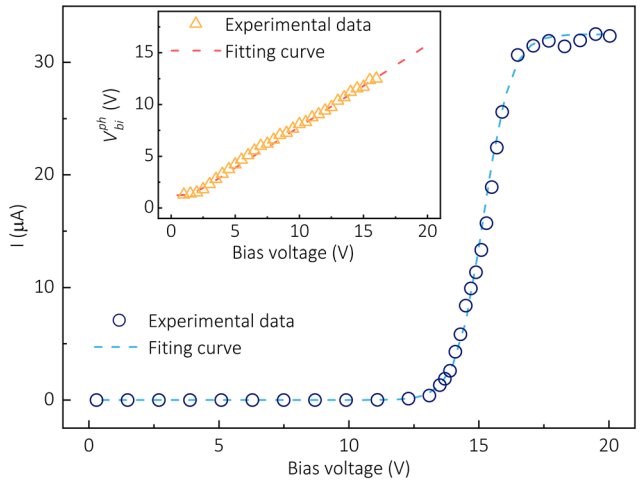

FIG. 4. Fitting curves showing the discharge photocurrent with bias voltage applied, where $v_r = 0.001$ V/s, $P_{\text{opt}} = 1$ mW/cm^2, and $t_e = 1$ s. Inset: the linear relation between V_{bi}^{ph} and V after full optical charging, where $v_r = 0.1$ V/s, $P_{\text{opt}} = 5\ \mu$W/cm^2, and $t_e = 6$ s.

As the first CPC device, the WSe_2-Q2DEG heterostructure shows the potential applications for optical memory, optical information, and self-excited devices. One crucial advantage of the CPC effect is the ability to achieve the conversion and storage of photocarriers simultaneously. Until now, no photoelectric devices that implement such functionality have been developed before this work (see Sec. 14 in the Supplemental Material [34]). Due to the infinite lifetime of the photocarriers stored in ISCR, randomly scattered photons in the environment may be gathered and harvested gradually so as to generate a large photocurrent.

In summary, WSe_2-Q2DEG heterostructure-based CPC devices show promise for high-efficiency photoelectric conversion and energy storage. Our experiments demonstrate that the infinite-lifetime photocarriers and insulating p-n interface are two key factors in determining the CPC effect. Further, the photocarriers can be completely self-excited and gradually accumulated without loss, and we have built a theoretical model to explain this striking effect. Our work opens up new opportunities to achieve a high-performance collection of optical information with multiple benefits for future memory and energy applications.

This work has been supported by the National Natural Science Foundation of China (Grants No. 11504254, No. 11704272, No. 11974304, No. 61805159, No. 12074282, and No. 62004136). This work is also supported by the Natural Science Foundation of the Jiangsu Higher Education Institutions of China (18KJB430023), Fund of Shanghai Natural Science Foundation (Grant No. 18ZR1445800), Natural Science Foundation of Jiangsu Province (BK20180970), and the Guangdong Natural Science Funds (2019A1515011007). C. W. Q. is supported by the National Research Foundation, Prime Minister's Office, Singapore, under Competitive Research Program Award NRF-CRP22-2019-0006.

*Corresponding author.
jyc@usts.edu.cn
†Corresponding author.
chengwei.qiu@nus.edu.sg
‡A. H. has the same contribution as Y. J.

[1] W. Shockley and H. J. Queisser, J. Appl. Phys. **32**, 510 (1961).
[2] E. A. Davis and N. F. Mott, Philos. Mag. **22**, 0903 (1970).
[3] O. E. Semonin, J. M. Luther, S. Choi, H.-Y. Chen, J. Gao, A. J. Nozik, and M. C. Beard, Science **334**, 1530 (2011).
[4] R. C. Alig and S. Bloom, Phys. Rev. Lett. **35**, 1522 (1975).
[5] M. O'Neil, J. Marohn, and G. McLendon, J. Phys. Chem. **94**, 4356 (1990).

[6] J. Burschka, N. Pellet, S.-J. Moon, R. Humphry-Baker, P. Gao, M. K. Nazeeruddin, and M. Grätzel, Nature (London) **499**, 316 (2013).
[7] M. A. Green, A. Ho-Baillie, and H. J. Snaith, Nat. Photonics **8**, 506 (2014).
[8] H. Zhou, Q. Chen, G. Li, S. Luo, T.-B. Song, H.-S. Duan, Z. Hong, J. You, Y. Liu, and Y. Yang, Science **345**, 542 (2014).
[9] H. Lu, W. Tian, F. Cao, Y. Ma, B. Gu, and L. Li, Adv. Funct. Mater. **26**, 1296 (2016).
[10] W. L. Barnes, A. Dereux, and T. W. Ebbesen, Nature (London) **424**, 824 (2003).
[11] D. M. Schaadt, B. Feng, and E. T. Yu, Appl. Phys. Lett. **86**, 063106 (2005).
[12] H. A. Atwater and A. Polman, Nat. Mater. **9**, 205 (2010).
[13] S. Pillai, K. R. Catchpole, T. Trupke, and M. A. Green, J. Appl. Phys. **101**, 093105 (2007).
[14] P. Jackson, R. Wuerz, D. Hariskos, E. Lotter, W. Witte, and M. Powalla, Phys. Status Solidi-R **10**, 583 (2016).
[15] Q. Liu, Y. Zhou, Y. Duan, M. Wang, and Y. Lin, Electrochim. Acta **95**, 48 (2013).
[16] Y. Liu, N. O. Weiss, X. Duan, H.-C. Cheng, Y. Huang, and X. Duan, Nat. Rev. Mater. **1**, 16042 (2016).
[17] A. Nourbakhsh, A. Zubair, M. S. Dresselhaus, and T. Palacios, Nano Lett. **16**, 1359 (2016).
[18] D. Jariwala, T. J. Marks, and M. C. Hersam, Nat. Mater. **16**, 170 (2017).
[19] J. Ran, W. Guo, H. Wang, B. Zhu, J. Yu, and S.-Z. Qiao, Adv. Mater. **30**, 1800128 (2018).
[20] A. K. Geim and I. V. Grigorieva, Nature (London) **499**, 419 (2013).
[21] K. S. Novoselov, A. Mishchenko, A. Carvalho, and A. H. Castro Neto, Science **353**, aac9439 (2016).
[22] Y. T. Lee *et al.*, Adv. Funct. Mater. **27**, 1703822 (2017).
[23] H. Yuan *et al.*, Nat. Nanotechnol. **9**, 851 (2014).
[24] S. Y. Xu *et al.*, Nat. Phys. **14**, 900 (2018).
[25] M. Massicotte, P. Schmidt, F. Vialla, K. G. Schädler, A. Reserbat-Plantey, K. Watanabe, T. Taniguchi, K. J. Tielrooij, and F. H. L. Koppens, Nat. Nanotechnol. **11**, 42 (2016).
[26] M. M. Furchi, A. Pospischil, F. Libisch, J. Burgdörfer, and T. Mueller, Nano Lett. **14**, 4785 (2014).
[27] C.-H. Lee *et al.*, Nat. Nanotechnol. **9**, 676 (2014).
[28] Y. J. Zhang, T. Ideue, M. Onga, F. Qin, R. Suzuki, A. Zak, R. Tenne, J. H. Smet, and Y. Iwasa, Nature (London) **570**, 349 (2019).
[29] F. Withers *et al.*, Nat. Mater. **14**, 301 (2015).
[30] K. F. Mak, C. Lee, J. Hone, J. Shan, and T. F. Heinz, Phys. Rev. Lett. **105**, 136805 (2010).
[31] A. Ohtomo and H. Y. Hwang, Nature (London) **427**, 423 (2004).
[32] G. Z. Liu, J. Qiu, Y. C. Jiang, R. Zhao, J. L. Yao, M. Zhao, Y. Feng, and J. Gao, Appl. Phys. Lett. **109**, 031110 (2016).
[33] G. Z. Liu, R. Zhao, J. Qiu, Y. C. Jiang, and J. Gao, J. Phys. D Appl. Phys. **52**, 095302 (2019).
[34] See Supplemental Material http://link.aps.org/supplemental/10.1103/PhysRevLett.127.217401 for the details of the device fabrication, the charging and discharging processes of photocarriers and the discussion in theoretical model, which includes Refs. [35–38].
[35] V. K. Guduru *et al.*, Appl. Phys. Lett. **102**, 051604 (2013).
[36] N. R. Pradhan *et al.*, Sci. Rep. **5**, 8979 (2015).
[37] A. P. He, Y. C. Jiang, J. Q. Chen, R. Zhao, G. Z. Liu, and J. Gao, J. Phys. D Appl. Phys. **52**, 375303 (2019).
[38] D. J. Groenendijk, M. Buscema, G. A. Steele, S. Michaelis de Vasconcellos, R. Bratschitsch, H. S. J. van der Zant, and A. Castellanos-Gomez, Nano Lett. **14**, 5846 (2014).
[39] D. W. Reagor and V. Y. Butko, Nat. Mater. **4**, 593 (2005).
[40] G. Herranz *et al.*, J. Appl. Phys. **107**, 103704 (2010).
[41] W. J. Zhao, Z. Ghorannevis, L. Q. Chu, M. L. Toh, C. Kloc, P.-H. Tan, and G. Eda, ACS Nano **7**, 791 (2013).
[42] G. W. Mudd *et al.*, Adv. Mater. **27**, 3760 (2015).
[43] H.-Y. Chen, M. K. F. Lo, G. W. Yang, H. G. Monbouquette, and Y. Yang, Nat. Nanotechnol. **3**, 543 (2008).
[44] W. C. Tan, L. Huang, R. J. Ng, L. Wang, D. M. N. Hasan, T. J. Duffin, K. S. Kumar, C. A. Nijhuis, C. Lee, and K.-W. Ang, Adv. Mater. **30**, 1705039 (2018).